Measurement of $\psi(3686) \to \Lambda\bar{\Lambda}\eta$ and $\psi(3686) \to \Lambda\bar{\Lambda}\pi^0$ decays

M. Ablikim,[1] M. N. Achasov,[11,b] P. Adlarson,[70] M. Albrecht,[4] R. Aliberti,[31] A. Amoroso,[69a,69c] M. R. An,[35] Q. An,[66,53] X. H. Bai,[61] Y. Bai,[52] O. Bakina,[32] R. Baldini Ferroli,[26a] I. Balossino,[1,27a] Y. Ban,[42,g] V. Batozskaya,[1,40] D. Becker,[31] K. Begzsuren,[29] N. Berger,[31] M. Bertani,[26a] D. Bettoni,[27a] F. Bianchi,[69a,69c] J. Bloms,[63] A. Bortone,[69a,69c] I. Boyko,[32] R. A. Briere,[5] A. Brueggemann,[63] H. Cai,[71] X. Cai,[1,53] A. Calcaterra,[26a] G. F. Cao,[1,58] N. Cao,[1,58] S. A. Cetin,[57a] J. F. Chang,[1,53] W. L. Chang,[1,58] G. Chelkov,[32,a] C. Chen,[39] Chao Chen,[50] G. Chen,[1] H. S. Chen,[1,58] M. L. Chen,[1,53] S. J. Chen,[38] S. M. Chen,[56] T. Chen,[1] X. R. Chen,[28,58] X. T. Chen,[1] Y. B. Chen,[1,53] Z. J. Chen,[23,h] W. S. Cheng,[69c] S. K. Choi,[50] X. Chu,[39] G. Cibinetto,[27a] F. Cossio,[69c] J. J. Cui,[45] H. L. Dai,[1,53] J. P. Dai,[73] A. Dbeyssi,[17] R. E. de Boer,[4] D. Dedovich,[32] Z. Y. Deng,[1] A. Denig,[31] I. Denysenko,[32] M. Destefanis,[69a,69c] F. De Mori,[69a,69c] Y. Ding,[36] J. Dong,[1,53] L. Y. Dong,[1,58] M. Y. Dong,[1,53,58] X. Dong,[71] S. X. Du,[75] P. Egorov,[32,a] Y. L. Fan,[71] J. Fang,[1,53] S. S. Fang,[1,58] W. X. Fang,[1] Y. Fang,[1] R. Farinelli,[27a] L. Fava,[69b,69c] F. Feldbauer,[4] G. Felici,[26a] C. Q. Feng,[66,53] J. H. Feng,[54] K. Fischer,[64] M. Fritsch,[4] C. Fritzsch,[63] C. D. Fu,[1] H. Gao,[58] Y. N. Gao,[42,g] Yang Gao,[66,53] S. Garbolino,[69c] I. Garzia,[27a,27b] P. T. Ge,[71] Z. W. Ge,[38] C. Geng,[54] E. M. Gersabeck,[62] A. Gilman,[64] K. Goetzen,[12] L. Gong,[36] W. X. Gong,[1,53] W. Gradl,[31] M. Greco,[69a,69c] L. M. Gu,[38] M. H. Gu,[1,53] Y. T. Gu,[14] C. Y. Guan,[1,58] A. Q. Guo,[28,58] L. B. Guo,[37] R. P. Guo,[44] Y. P. Guo,[10,f] A. Guskov,[32,a] T. T. Han,[45] W. Y. Han,[35] X. Q. Hao,[18] F. A. Harris,[60] K. K. He,[50] K. L. He,[1,58] F. H. Heinsius,[4] C. H. Heinz,[31] Y. K. Heng,[1,53,58] C. Herold,[55] M. Himmelreich,[31,d] G. Y. Hou,[1,58] Y. R. Hou,[58] Z. L. Hou,[1] H. M. Hu,[1,58] J. F. Hu,[51,i] T. Hu,[1,53,58] Y. Hu,[1] G. S. Huang,[66,53] K. X. Huang,[54] L. Q. Huang,[67] L. Q. Huang,[28,58] X. T. Huang,[45] Y. P. Huang,[1] Z. Huang,[42,g] T. Hussain,[68] N. Hüsken,[25,31] W. Imoehl,[25] M. Irshad,[66,53] J. Jackson,[25] S. Jaeger,[4] S. Janchiv,[29] E. Jang,[50] J. H. Jeong,[50] Q. Ji,[1] Q. P. Ji,[18] X. B. Ji,[1,58] X. L. Ji,[1,53] Y. Y. Ji,[45] Z. K. Jia,[66,53] H. B. Jiang,[45] S. S. Jiang,[35] X. S. Jiang,[1,53,58] Y. Jiang,[58] J. B. Jiao,[45] Z. Jiao,[21] S. Jin,[38] Y. Jin,[61] M. Q. Jing,[1,58] T. Johansson,[70] N. Kalantar-Nayestanaki,[59] X. S. Kang,[36] R. Kappert,[59] M. Kavatsyuk,[59] B. C. Ke,[75] I. K. Keshk,[4] A. Khoukaz,[63] P. Kiese,[31] R. Kiuchi,[1] R. Kliemt,[12] L. Koch,[33] O. B. Kolcu,[57a] B. Kopf,[4] M. Kuemmel,[4] M. Kuessner,[4] A. Kupsc,[40,70] W. Kühn,[33] J. J. Lane,[62] J. S. Lange,[33] P. Larin,[17] A. Lavania,[24] L. Lavezzi,[69a,69c] Z. H. Lei,[66,53] H. Leithoff,[31] M. Lellmann,[31] T. Lenz,[31] C. Li,[43] C. Li,[39] C. H. Li,[35] Cheng Li,[66,53] D. M. Li,[75] F. Li,[1,53] G. Li,[1] H. Li,[47] H. Li,[66,53] H. B. Li,[1,58] H. J. Li,[18] H. N. Li,[51,i] J. Q. Li,[4] J. S. Li,[54] J. W. Li,[45] Ke Li,[1] L. J. Li,[1] L. K. Li,[1] Lei Li,[3] M. H. Li,[39] P. R. Li,[34,j,k] S. X. Li,[10] S. Y. Li,[56] T. Li,[45] W. D. Li,[1,58] W. G. Li,[1] X. H. Li,[66,53] X. L. Li,[45] Xiaoyu Li,[1,58] H. Liang,[66,53] H. Liang,[1,58] H. Liang,[30] Y. F. Liang,[49] Y. T. Liang,[28,58] G. R. Liao,[13] L. Z. Liao,[45] J. Libby,[24] A. Limphirat,[55] C. X. Lin,[54] D. X. Lin,[28,58] T. Lin,[1] B. J. Liu,[1] C. X. Liu,[1] D. Liu,[17,66] F. H. Liu,[48] Fang Liu,[1] Feng Liu,[6] G. M. Liu,[51,i] H. Liu,[34,j,k] H. B. Liu,[14] H. M. Liu,[1,58] Huanhuan Liu,[1] Huihui Liu,[19] J. B. Liu,[66,53] J. L. Liu,[67] J. Y. Liu,[1,58] K. Liu,[1] K. Y. Liu,[36] Ke Liu,[20] L. Liu,[66,53] M. H. Liu,[10,f] P. L. Liu,[1] Q. Liu,[58] S. B. Liu,[66,53] T. Liu,[10,f] W. K. Liu,[39] W. M. Liu,[66,53] X. Liu,[34,j,k] Y. Liu,[34,j,k] Y. B. Liu,[39] Z. A. Liu,[1,53,58] Z. Q. Liu,[45] X. C. Lou,[1,53,58] F. X. Lu,[54] H. J. Lu,[21] J. G. Lu,[1,53] X. L. Lu,[1] Y. Lu,[7] Y. P. Lu,[1,53] Z. H. Lu,[1] C. L. Luo,[37] M. X. Luo,[74] T. Luo,[10,f] X. L. Luo,[1,53] X. R. Lyu,[58] Y. F. Lyu,[39] F. C. Ma,[36] H. L. Ma,[1] L. L. Ma,[45] M. M. Ma,[1,58] Q. M. Ma,[1] R. Q. Ma,[1,58] R. T. Ma,[58] X. Y. Ma,[1,53] Y. Ma,[42,g] F. E. Maas,[17] M. Maggiora,[69a,69c] S. Maldaner,[4] S. Malde,[64] Q. A. Malik,[68] A. Mangoni,[26b] Y. J. Mao,[42,g] Z. P. Mao,[1] S. Marcello,[69a,69c] Z. X. Meng,[61] J. G. Messchendorp,[59,12] G. Mezzadri,[1,27a] H. Miao,[1] T. J. Min,[38] R. E. Mitchell,[25] X. H. Mo,[1,53,58] N. Yu. Muchnoi,[11,b] Y. Nefedov,[32] F. Nerling,[17,d] I. B. Nikolaev,[11] Z. Ning,[1,53] S. Nisar,[9,l] Y. Niu,[45] S. L. Olsen,[58] Q. Ouyang,[1,53,58] S. Pacetti,[26b,26c] X. Pan,[10,f] Y. Pan,[52] A. Pathak,[1] A. Pathak,[30] M. Pelizaeus,[4] H. P. Peng,[66,53] K. Peters,[12,d] J. Pettersson,[70] J. L. Ping,[37] R. G. Ping,[1,58] S. Plura,[31] S. Pogodin,[32] V. Prasad,[66,53] F. Z. Qi,[1] H. Qi,[66,53] H. R. Qi,[56] M. Qi,[38] T. Y. Qi,[10,f] S. Qian,[1,53] W. B. Qian,[58] Z. Qian,[54] C. F. Qiao,[58] J. J. Qin,[67] L. Q. Qin,[13] X. P. Qin,[10,f] X. S. Qin,[45] Z. H. Qin,[1,53] J. F. Qiu,[1] S. Q. Qu,[39] S. Q. Qu,[56] K. H. Rashid,[68] C. F. Redmer,[31] K. J. Ren,[35] A. Rivetti,[69c] V. Rodin,[59] M. Rolo,[69c] G. Rong,[1,58] Ch. Rosner,[17] S. N. Ruan,[39] H. S. Sang,[66] A. Sarantsev,[32,c] Y. Schelhaas,[31] C. Schnier,[4] K. Schönning,[70] M. Scodeggio,[27a,27b] K. Y. Shan,[10,f] W. Shan,[22] X. Y. Shan,[66,53] J. F. Shangguan,[50] L. G. Shao,[1,58] M. Shao,[66,53] C. P. Shen,[10,f] H. F. Shen,[1,58] X. Y. Shen,[1,58] B.-A. Shi,[58] H. C. Shi,[66,53] J. Y. Shi,[1] Q. Q. Shi,[50] R. S. Shi,[1,58] X. Shi,[1,53] X. D. Shi,[66,53] J. J. Song,[18] W. M. Song,[1,30] Y. X. Song,[42,g] S. Sosio,[69a,69c] S. Spataro,[69a,69c] F. Stieler,[31] K. X. Su,[71] P. P. Su,[50] Y.-J. Su,[58] G. X. Sun,[1] H. Sun,[58] H. K. Sun,[1] J. F. Sun,[18] L. Sun,[71] S. S. Sun,[1,58] T. Sun,[1,58] W. Y. Sun,[30] X. Sun,[23,h] Y. J. Sun,[66,53] Y. Z. Sun,[1] Z. T. Sun,[45] Y. H. Tan,[71] Y. X. Tan,[66,53] C. J. Tang,[49] G. Y. Tang,[1] J. Tang,[54] L. Y. Tao,[67] Q. T. Tao,[23,h] M. Tat,[64] J. X. Teng,[66,53] V. Thoren,[70] W. H. Tian,[47] Y. Tian,[28,58] I. Uman,[57b] B. Wang,[1] B. L. Wang,[58] C. W. Wang,[38] D. Y. Wang,[42,g] F. Wang,[67] H. J. Wang,[34,j,k] H. P. Wang,[1,58] K. Wang,[1,53] L. L. Wang,[1] M. Wang,[45] M. Z. Wang,[42,g] Meng Wang,[1,58] S. Wang,[10,f] S. Wang,[13] T. Wang,[10,f] T. J. Wang,[39] W. Wang,[54] W. H. Wang,[71] W. P. Wang,[66,53] X. Wang,[42,g] X. F. Wang,[34,j,k] X. L. Wang,[10,f] Y. D. Wang,[41] Y. F. Wang,[1,53,58] Y. H. Wang,[43] Y. Q. Wang,[1] Yaqian Wang,[1,16] Y. Wang,[56] Z. Wang,[1,53] Z. Y. Wang,[1,58] Ziyi Wang,[58] D. H. Wei,[13] F. Weidner,[63] S. P. Wen,[1] D. J. White,[62] U. Wiedner,[4] G. Wilkinson,[64] M. Wolke,[70] L. Wollenberg,[4] J. F. Wu,[1,58] L. H. Wu,[1] L. J. Wu,[1,58] X. Wu,[10,f] X. H. Wu,[30] Y. Wu,[66] Z. Wu,[1,53] L. Xia,[66,53] T. Xiang,[42,g] D. Xiao,[34,j,k] G. Y. Xiao,[38] H. Xiao,[10,f] S. Y. Xiao,[1] Y. L. Xiao,[10,f] Z. J. Xiao,[37]

C. Xie,[38] X. H. Xie,[42,g] Y. Xie,[45] Y. G. Xie,[1,53] Y. H. Xie,[6] Z. P. Xie,[66,53] T. Y. Xing,[1,58] C. F. Xu,[1] C. J. Xu,[54] G. F. Xu,[1] H. Y. Xu,[61] Q. J. Xu,[15] S. Y. Xu,[65] X. P. Xu,[50] Y. C. Xu,[58] Z. P. Xu,[38] F. Yan,[10,f] L. Yan,[10,f] W. B. Yan,[66,53] W. C. Yan,[75] H. J. Yang,[46,e] H. L. Yang,[30] H. X. Yang,[1] L. Yang,[47] S. L. Yang,[58] Tao Yang,[1] Y. F. Yang,[39] Y. X. Yang,[1,58] Yifan Yang,[1,58] M. Ye,[1,53] M. H. Ye,[8] J. H. Yin,[1] Z. Y. You,[54] B. X. Yu,[1,53,58] C. X. Yu,[39] G. Yu,[1,58] T. Yu,[67] C. Z. Yuan,[1,58] L. Yuan,[2] S. C. Yuan,[1] X. Q. Yuan,[1] Y. Yuan,[1,58] Z. Y. Yuan,[54] C. X. Yue,[35] A. A. Zafar,[68] F. R. Zeng,[45] X. Zeng,[6] Y. Zeng,[23,h] Y. H. Zhan,[54] A. Q. Zhang,[1] B. L. Zhang,[1] B. X. Zhang,[1] D. H. Zhang,[39] G. Y. Zhang,[18] H. Zhang,[66] H. H. Zhang,[54] H. H. Zhang,[30] H. Y. Zhang,[1,53] J. L. Zhang,[72] J. Q. Zhang,[37] J. W. Zhang,[1,53,58] J. X. Zhang,[34,j,k] J. Y. Zhang,[1] J. Z. Zhang,[1,58] Jianyu Zhang,[1,58] Jiawei Zhang,[1,58] L. M. Zhang,[56] L. Q. Zhang,[54] Lei Zhang,[38] P. Zhang,[1] Q. Y. Zhang,[35,75] Shulei Zhang,[23,h] X. D. Zhang,[41] X. M. Zhang,[1] X. Y. Zhang,[45] X. Y. Zhang,[50] Y. Zhang,[64] Y. T. Zhang,[75] Y. H. Zhang,[1,53] Yan Zhang,[66,53] Yao Zhang,[1] Z. H. Zhang,[1] Z. Y. Zhang,[71] Z. Y. Zhang,[39] G. Zhao,[1] J. Zhao,[35] J. Y. Zhao,[1,58] J. Z. Zhao,[1,53] Lei Zhao,[66,53] Ling Zhao,[1] M. G. Zhao,[39] Q. Zhao,[1] S. J. Zhao,[75] Y. B. Zhao,[1,53] Y. X. Zhao,[28,58] Z. G. Zhao,[66,53] A. Zhemchugov,[32,a] B. Zheng,[67] J. P. Zheng,[1,53] Y. H. Zheng,[58] B. Zhong,[37] C. Zhong,[67] X. Zhong,[54] H. Zhou,[45] L. P. Zhou,[1,58] X. Zhou,[71] X. K. Zhou,[58] X. R. Zhou,[66,53] X. Y. Zhou,[35] Y. Z. Zhou,[10,f] J. Zhu,[39] K. Zhu,[1] K. J. Zhu,[1,53,58] L. X. Zhu,[58] S. H. Zhu,[65] S. Q. Zhu,[38] T. J. Zhu,[72] W. J. Zhu,[10,f] Y. C. Zhu,[66,53] Z. A. Zhu,[1,58] B. S. Zou,[1] and J. H. Zou[1]

(BESIII Collaboration)

[1]*Institute of High Energy Physics, Beijing 100049, People's Republic of China*
[2]*Beihang University, Beijing 100191, People's Republic of China*
[3]*Beijing Institute of Petrochemical Technology, Beijing 102617, People's Republic of China*
[4]*Bochum Ruhr-University, D-44780 Bochum, Germany*
[5]*Carnegie Mellon University, Pittsburgh, Pennsylvania 15213, USA*
[6]*Central China Normal University, Wuhan 430079, People's Republic of China*
[7]*Central South University, Changsha 410083, People's Republic of China*
[8]*China Center of Advanced Science and Technology, Beijing 100190, People's Republic of China*
[9]*COMSATS University Islamabad, Lahore Campus, Defence Road, Off Raiwind Road, 54000 Lahore, Pakistan*
[10]*Fudan University, Shanghai 200433, People's Republic of China*
[11]*G.I. Budker Institute of Nuclear Physics SB RAS (BINP), Novosibirsk 630090, Russia*
[12]*GSI Helmholtzcentre for Heavy Ion Research GmbH, D-64291 Darmstadt, Germany*
[13]*Guangxi Normal University, Guilin 541004, People's Republic of China*
[14]*Guangxi University, Nanning 530004, People's Republic of China*
[15]*Hangzhou Normal University, Hangzhou 310036, People's Republic of China*
[16]*Hebei University, Baoding 071002, People's Republic of China*
[17]*Helmholtz Institute Mainz, Staudinger Weg 18, D-55099 Mainz, Germany*
[18]*Henan Normal University, Xinxiang 453007, People's Republic of China*
[19]*Henan University of Science and Technology, Luoyang 471003, People's Republic of China*
[20]*Henan University of Technology, Zhengzhou 450001, People's Republic of China*
[21]*Huangshan College, Huangshan 245000, People's Republic of China*
[22]*Hunan Normal University, Changsha 410081, People's Republic of China*
[23]*Hunan University, Changsha 410082, People's Republic of China*
[24]*Indian Institute of Technology Madras, Chennai 600036, India*
[25]*Indiana University, Bloomington, Indiana 47405, USA*
[26a]*INFN Laboratori Nazionali di Frascati, I-00044, Frascati, Italy*
[26b]*INFN Sezione di Perugia, I-06100, Perugia, Italy*
[26c]*University of Perugia, I-06100 Perugia, Italy*
[27a]*INFN Sezione di Ferrara, I-44122, Ferrara, Italy*
[27b]*University of Ferrara, I-44122 Ferrara, Italy*
[28]*Institute of Modern Physics, Lanzhou 730000, People's Republic of China*
[29]*Institute of Physics and Technology, Peace Ave. 54B, Ulaanbaatar 13330, Mongolia*
[30]*Jilin University, Changchun 130012, People's Republic of China*
[31]*Johannes Gutenberg University of Mainz, Johann-Joachim-Becher-Weg 45, D-55099 Mainz, Germany*
[32]*Joint Institute for Nuclear Research, 141980 Dubna, Moscow region, Russia*
[33]*Justus-Liebig-Universitaet Giessen, II. Physikalisches Institut, Heinrich-Buff-Ring 16, D-35392 Giessen, Germany*
[34]*Lanzhou University, Lanzhou 730000, People's Republic of China*
[35]*Liaoning Normal University, Dalian 116029, People's Republic of China*
[36]*Liaoning University, Shenyang 110036, People's Republic of China*
[37]*Nanjing Normal University, Nanjing 210023, People's Republic of China*

[38]*Nanjing University, Nanjing 210093, People's Republic of China*
[39]*Nankai University, Tianjin 300071, People's Republic of China*
[40]*National Centre for Nuclear Research, Warsaw 02-093, Poland*
[41]*North China Electric Power University, Beijing 102206, People's Republic of China*
[42]*Peking University, Beijing 100871, People's Republic of China*
[43]*Qufu Normal University, Qufu 273165, People's Republic of China*
[44]*Shandong Normal University, Jinan 250014, People's Republic of China*
[45]*Shandong University, Jinan 250100, People's Republic of China*
[46]*Shanghai Jiao Tong University, Shanghai 200240, People's Republic of China*
[47]*Shanxi Normal University, Linfen 041004, People's Republic of China*
[48]*Shanxi University, Taiyuan 030006, People's Republic of China*
[49]*Sichuan University, Chengdu 610064, People's Republic of China*
[50]*Soochow University, Suzhou 215006, People's Republic of China*
[51]*South China Normal University, Guangzhou 510006, People's Republic of China*
[52]*Southeast University, Nanjing 211100, People's Republic of China*
[53]*State Key Laboratory of Particle Detection and Electronics, Beijing 100049, Hefei 230026, People's Republic of China*
[54]*Sun Yat-Sen University, Guangzhou 510275, People's Republic of China*
[55]*Suranaree University of Technology, University Avenue 111, Nakhon Ratchasima 30000, Thailand*
[56]*Tsinghua University, Beijing 100084, People's Republic of China*
[57a]*Turkish Accelerator Center Particle Factory Group, Istinye University, 34010 Istanbul, Turkey*
[57b]*Turkish Accelerator Center Particle Factory Group, Near East University, Nicosia, North Cyprus, Mersin 10, Turkey*
[58]*University of Chinese Academy of Sciences, Beijing 100049, People's Republic of China*
[59]*University of Groningen, NL-9747 AA Groningen, The Netherlands*
[60]*University of Hawaii, Honolulu, Hawaii 96822, USA*
[61]*University of Jinan, Jinan 250022, People's Republic of China*
[62]*University of Manchester, Oxford Road, Manchester M13 9PL, United Kingdom*
[63]*University of Muenster, Wilhelm-Klemm-Str. 9, 48149 Muenster, Germany*
[64]*University of Oxford, Keble Rd, Oxford OX13RH, United Kingdom*
[65]*University of Science and Technology Liaoning, Anshan 114051, People's Republic of China*
[66]*University of Science and Technology of China, Hefei 230026, People's Republic of China*
[67]*University of South China, Hengyang 421001, People's Republic of China*
[68]*University of the Punjab, Lahore-54590, Pakistan*
[69a]*University of Turin, I-10125 Turin, Italy*
[69b]*University of Eastern Piedmont, I-15121, Alessandria, Italy*
[69c]*INFN, I-10125 Turin, Italy*
[70]*Uppsala University, Box 516, SE-75120 Uppsala, Sweden*
[71]*Wuhan University, Wuhan 430072, People's Republic of China*
[72]*Xinyang Normal University, Xinyang 464000, People's Republic of China*
[73]*Yunnan University, Kunming 650500, People's Republic of China*
[74]*Zhejiang University, Hangzhou 310027, People's Republic of China*
[75]*Zhengzhou University, Zhengzhou 450001, People's Republic of China*

(Received 1 August 2022; accepted 7 September 2022; published 19 October 2022; corrected 26 October 2022)

[a]Also at the Moscow Institute of Physics and Technology, Moscow 141700, Russia.
[b]Also at the Novosibirsk State University, Novosibirsk 630090, Russia.
[c]Also at the NRC "Kurchatov Institute", PNPI, 188300 Gatchina, Russia.
[d]Also at Goethe University Frankfurt, 60323 Frankfurt am Main, Germany.
[e]Also at Key Laboratory for Particle Physics, Astrophysics and Cosmology, Ministry of Education; Shanghai Key Laboratory for Particle Physics and Cosmology; Institute of Nuclear and Particle Physics, Shanghai 200240, People's Republic of China.
[f]Also at Key Laboratory of Nuclear Physics and Ion-beam Application (MOE) and Institute of Modern Physics, Fudan University, Shanghai 200443, People's Republic of China.
[g]Also at State Key Laboratory of Nuclear Physics and Technology, Peking University, Beijing 100871, People's Republic of China.
[h]Also at School of Physics and Electronics, Hunan University, Changsha 410082, China.
[i]Also at Guangdong Provincial Key Laboratory of Nuclear Science, Institute of Quantum Matter, South China Normal University, Guangzhou 510006, China.
[j]Also at Frontiers Science Center for Rare Isotopes, Lanzhou University, Lanzhou 730000, People's Republic of China.
[k]Also at Lanzhou Center for Theoretical Physics, Lanzhou University, Lanzhou 730000, People's Republic of China.
[l]Also at the Department of Mathematical Sciences, IBA, Karachi, Pakistan.

Based on a sample of 448.1×10^6 $\psi(3686)$ events collected with the BESIII detector, a study of $\psi(3686) \to \Lambda\bar{\Lambda}\pi^0$ and $\psi(3686) \to \Lambda\bar{\Lambda}\eta$ is performed. Evidence of the isospin-violating decay $\psi(3686) \to \Lambda\bar{\Lambda}\pi^0$ is found for the first time with a statistical significance of 3.7σ, the branching fraction $\mathcal{B}(\psi(3686) \to \Lambda\bar{\Lambda}\pi^0)$ is measured to be $(1.42 \pm 0.39 \pm 0.59) \times 10^{-6}$, and its corresponding upper limit is determined to be 2.47×10^{-6} at 90% confidence level. A partial wave analysis of $\psi(3686) \to \Lambda\bar{\Lambda}\eta$ shows that the peak around $\Lambda\eta$ invariant mass threshold favors a Λ^* resonance with mass and width in agreement with the $\Lambda(1670)$. The branching fraction of the $\psi(3686) \to \Lambda\bar{\Lambda}\eta$ is measured to be $(2.34 \pm 0.18 \pm 0.52) \times 10^{-5}$. The first uncertainties are statistical and the second are systematic.

DOI: 10.1103/PhysRevD.106.072006

I. INTRODUCTION

The $\psi(3686)$ is the first radial excitation of the isospin singlet $c\bar{c}$ vector state, and its decays involving baryon pairs not only provide an opportunity to study the baryon structure, but also offer a unique place to investigate SU(3) flavor symmetry breaking effects. Using a sample of 107 million $\psi(3686)$ events collected in 2009, BESIII published a study investigating the reactions of $\psi(3686) \to \Lambda\bar{\Lambda}\pi^0$ and $\psi(3686) \to \Lambda\bar{\Lambda}\eta$ [1]. However, no significant signal for $\psi(3686) \to \Lambda\bar{\Lambda}\pi^0$ was seen, due to suppression from isospin conservation, and an upper limit of $\mathcal{B}(\psi(3686) \to \Lambda\bar{\Lambda}\pi^0) < 2.9 \times 10^{-6}$ was reported at the 90% confidence level (CL). Based on roughly 60 events, the first branching fraction measurement of $\psi(3686) \to \Lambda\bar{\Lambda}\eta$ was obtained: $\mathcal{B}(\psi(3686) \to \Lambda\bar{\Lambda}\eta) = (2.47 \pm 0.34 \pm 0.19) \times 10^{-5}$.

In 2012, another sample of $\psi(3686)$ events was collected at the BESIII detector [2]. The total data set of 448 million $\psi(3686)$ events, corresponding to a four-fold increase of 2009 data, allows for an in-depth investigation on the decays $\psi(3686) \to \Lambda\bar{\Lambda}\pi^0$ and $\psi(3686) \to \Lambda\bar{\Lambda}\eta$, and searches for intermediate Λ^* states in the $\Lambda\pi^0$ and $\Lambda\eta$ mass spectra. In addition, these branching fractions may also be used to test the "12%" rule [3–5], which predicts that the ratio of branching fractions of $\psi(3686)$ and J/ψ decays into the same light hadron final states is around 12%. In this paper, the charge-conjugate process is always implied unless explicitly mentioned.

II. DETECTOR AND MONTE CARLO SAMPLES

The BESIII detector [6] records symmetric e^+e^- collisions provided by the BEPCII storage ring [7], in the center-of-mass energy range from 2.0 GeV to 4.95 GeV, with a peak luminosity of 1×10^{33} cm^{-2} s^{-1} achieved at $\sqrt{s} = 3.77$ GeV. BESIII has collected large data samples in this energy region [8]. The cylindrical core of the BESIII detector covers 93% of the full solid angle and consists of a helium-based multilayer drift chamber (MDC), a plastic scintillator time-of-flight system (TOF), and a CsI(Tl) electromagnetic calorimeter (EMC), which are all enclosed in a superconducting solenoidal magnet providing a 1.0 T magnetic field. The solenoid is supported by an octagonal flux-return yoke equipped with resistive plate counter muon identification modules interleaved with steel. The charged-particle momentum resolution at 1 GeV/c is 0.5%, and the resolution of the specific energy loss dE/dx in the MDC is 6% for electrons from Bhabha scattering. The EMC measures photon energies with a resolution of 2.5% (5%) at 1 GeV in the barrel (end cap) region. The time resolution in the TOF barrel region is 68 ps, while that in the end cap region is 110 ps.

Simulated data samples produced with a GEANT4-based [9] Monte Carlo (MC) package, which includes the geometric description of the BESIII detector and the detector response, are used to optimize the event selection criteria, determine detection efficiencies and estimate backgrounds. The simulation models the beam energy spread and initial state radiation (ISR) in e^+e^- annihilations with the generator KKMC [10,11]. The inclusive MC sample aims to include all possible processes involving the production of the J/ψ and $\psi(3686)$ resonances, and the continuum processes incorporated in KKMC [10,11]. The known decay modes are modeled with EVTGEN [12,13] using branching fractions taken from the Particle Data Group (PDG) [14], and the remaining unknown charmonium decays are modeled with LUNDCHARM [15,16]. Final state radiation (FSR) from charged particles is incorporated using PHOTOS [17]. Signal MC samples of $\psi(3686) \to \Lambda\bar{\Lambda}\pi^0$ decays are generated with uniform phase space (PHSP), while $\psi(3686) \to \Lambda\bar{\Lambda}\eta$ decays are generated according to the results of the partial wave analysis reported later in this paper.

III. EVENT SELECTION

The processes $\psi(3686) \to \Lambda\bar{\Lambda}\pi^0$ and $\psi(3686) \to \Lambda\bar{\Lambda}\eta$ are reconstructed with $\Lambda \to p\pi^-$, $\bar{\Lambda} \to \bar{p}\pi^+$, $\pi^0 \to \gamma\gamma$, and

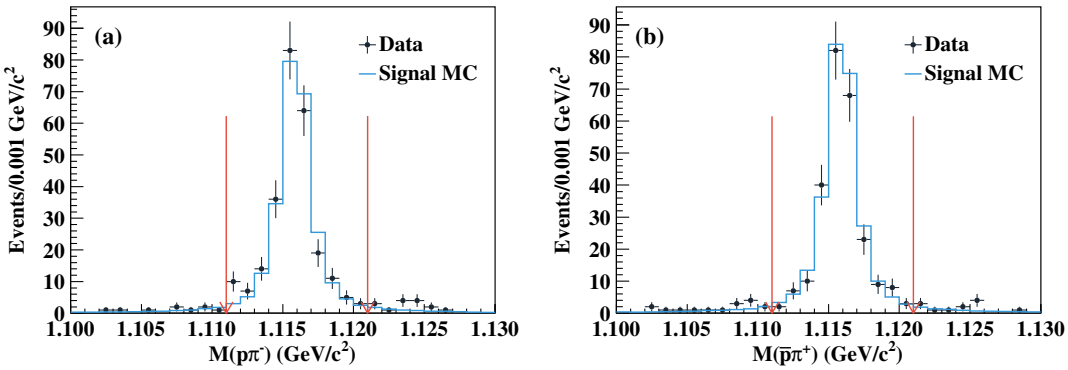

FIG. 1. The distributions of (a) $M(p\pi^-)$ and (b) $M(\bar{p}\pi^+)$. Dots with error bars represent data, the blue histograms are normalized signal MC. The mass window requirement of the $\Lambda(\bar{\Lambda})$ is shown with the red arrows.

$\eta \to \gamma\gamma$. Since the final state for both channels is $p\bar{p}\pi^+\pi^-\gamma\gamma$, the number of charged tracks is required to be four with net charge zero. Each track must satisfy $|\cos\theta| < 0.93$, where θ is the polar angle of the track measured by the MDC with respect to the direction of the positron beam.

Each of the photon candidates is required to have an energy deposit in the EMC of at least 25 MeV in the barrel ($|\cos\theta| < 0.80$) or 50 MeV in the end caps ($0.86 < |\cos\theta| < 0.92$). To eliminate showers from charged tracks, the angle between the position of each shower in the EMC and any charged track must be greater than 10 degrees. To suppress electronic noise and showers unrelated to the event, the EMC time difference from the event start time is required to be within [0, 700] ns. At least two photon candidates are required.

The Λ and $\bar{\Lambda}$ candidates are reconstructed by combining pairs of oppositely charged tracks with pion and proton mass hypotheses, fulfilling a secondary vertex constraint [18]. Events with at least one $p\pi^-(\Lambda)$ and one $\bar{p}\pi^+(\bar{\Lambda})$ candidate are selected. In the case of multiple $\Lambda\bar{\Lambda}$ pair candidates, the one with the minimum value of $\chi^2_{svtx}(\Lambda) + \chi^2_{svtx}(\bar{\Lambda})$ is chosen, where $\chi^2_{svtx}(\Lambda)$ and $\chi^2_{svtx}(\bar{\Lambda})$ are the fit qualities of the secondary vertex fits for Λ and $\bar{\Lambda}$, respectively. To improve the momentum and energy resolution and to reduce background contributions, a four-constraint (4C) energy-momentum conservation kinematic fit is applied to the event candidates under the hypothesis of $\Lambda\bar{\Lambda}\gamma\gamma$ (i.e., not considering the $\gamma\gamma$ mass), and the corresponding χ^2_{4C} is required to be less than 40. For events with more than two photon candidates, the combination with the best fit quality is selected from all possible combinations. To reject possible background contributions from $\psi(3686) \to \Lambda\bar{\Lambda}\gamma$ and $\psi(3686) \to \Lambda\bar{\Lambda}\gamma\gamma\gamma$, we further require that the χ^2 of the 4C fit for the $\psi(3686) \to \Lambda\bar{\Lambda}\gamma\gamma$ assignment is smaller than those of $\Lambda\bar{\Lambda}\gamma$ and $\Lambda\bar{\Lambda}\gamma\gamma\gamma$. The final $p\pi^-$ and $\bar{p}\pi^+$ mass distributions in two progresses are shown in Figs. 1(a) and 1(b), respectively, where clear Λ and $\bar{\Lambda}$ signals are visible.

We require that the invariant mass of $p\pi^-(\bar{p}\pi^+)$ should be in the mass region of Λ, $1.111 < M(p\pi^-, \bar{p}\pi^+) < 1.121$ GeV/c^2. To remove the background events from $\psi(3686) \to \pi^0(\eta)J/\psi$, $J/\psi \to \Lambda\bar{\Lambda}$, events with the invariant mass of $\Lambda\bar{\Lambda}$ in the J/ψ mass region, $3.087 < M(\Lambda\bar{\Lambda}) < 3.107$ GeV/c^2, are rejected. In order to suppress possible background events from $\psi(3686) \to \pi^+\pi^- J/\psi$ with $J/\psi \to p\bar{p}\pi^0(\eta)$, we reject events with $3.087 < M_{\rm rec}(\pi^+\pi^-) < 3.107$ GeV/c^2, where $M_{\rm rec}(\pi^+\pi^-)$ is the mass recoiling against the $\pi^+\pi^-$. No requirements on the $\gamma\gamma$ invariant mass are imposed since this is the variable which will be used to extract the signal yields.

In the case of $\psi(3686) \to \Lambda\bar{\Lambda}\pi^0$, additional requirements are applied to further reduce the contamination from background. The χ^2_{4C} is required to be less than 15, to further suppress background events with one or more than two photons in the final states. The veto cut $M(\Lambda\bar{\Lambda}) < 3.4$ GeV/c^2 is applied in order to suppress background from $\psi(3686) \to \Sigma^0\bar{\Sigma}^0$. Two other veto cuts, $M(p\pi^0, \bar{p}\pi^0) < 1.17$ GeV/c^2 and $M(p\pi^0, \bar{p}\pi^0) > 1.2$ GeV/c^2, are applied in order to suppress background from $\psi(3686) \to \Lambda\bar{\Sigma}^-\pi^+$. The invariant masses $M(\gamma_{\rm low}\Lambda)$ and $M(\gamma_{\rm low}\bar{\Lambda})$ are both required to be outside of $(1.183, 1.203)$ GeV/c^2 to suppress the $\psi(3686) \to \Lambda\bar{\Sigma}^0\pi^0$ background, where $\gamma_{\rm low}$ represents the less energetic candidate photon.

IV. BACKGROUND STUDY

To investigate the possible background contributions, the same selection criteria are applied to an inclusive MC sample of 506 million $\psi(3686)$ events. A topological analysis of the surviving events is performed with the generic tool TopoAna [19], and the results indicate that the background peaking at the π^0 invariant mass mainly comes from $\psi(3686) \to \Lambda\bar{\Sigma}^0\pi^0$, while the other background sources present a flat distribution. Thus, a PHSP MC sample of $\psi(3686) \to \Lambda\bar{\Sigma}^0\pi^0 + \text{c.c.}$ is generated, giving a background estimate of 20.4 ± 1.9 events, by using a branching fraction of $(1.54 \pm 0.04 \pm 0.13) \times 10^{-4}$

obtained from $\mathcal{B}(\psi(3686) \to \Lambda\bar{\Sigma}^{-}\pi^{+})$ with isospin symmetry considerations.

To estimate the background from e^+e^- continuum processes, the same procedure is performed on data taken at $\sqrt{s} = 3.773$ GeV, with an integrated luminosity of 2.92 fb^{-1} [20]. The background events are extracted by fitting the $M_{\gamma\gamma}$ mass distribution, normalized to the $\psi(3686)$ data taking into account the luminosity and energy-dependent cross section of the quantum electrodynamics (QED) processes. The normalization factor f is calculated as

$$f = \frac{N_{\psi(3686)}}{N_{\psi(3770)}} = \frac{\mathcal{L}_{\psi(3686)}}{\mathcal{L}_{\psi(3770)}} \cdot \frac{\sigma_{\psi(3686)}}{\sigma_{\psi(3770)}} \cdot \frac{\epsilon_{\psi(3686)}}{\epsilon_{\psi(3770)}},$$

where N, $\mathcal{L}$, σ, and ϵ refer to the number of observed events, integrated luminosity of data, cross section, and detection efficiency at the two center of mass energies, respectively. The details on the cross section values can be found in Ref. [21]. The detection efficiency ratio $\epsilon_{\psi(3686)}/\epsilon_{\psi(3770)}$ has been determined by Monte Carlo simulations. After normalization, the background contributions from $e^+e^- \to \Lambda\bar{\Lambda}\pi^0$ and $e^+e^- \to \Lambda\bar{\Lambda}\eta$ at 3.686 GeV are determined to be 13.2 ± 1.7 and 19.1 ± 2.0 events, respectively.

Due to the identical event topology, these background events are indistinguishable from signal events and are subtracted directly by fixing their magnitudes in the fit when extracting signal yields. Here we assume that the interference between $\psi(3686)$ decay and continuum process is negligible.

V. ANALYSIS OF $\psi(3686) \to \Lambda\bar{\Lambda}\pi^0$

The $\psi(3686) \to \Lambda\bar{\Lambda}\pi^0$ signal yield is obtained from an extended unbinned maximum likelihood fit to the $\gamma\gamma$ invariant mass distribution. The total probability density function consists of a signal and various background contributions. The signal component is modeled with the MC simulated signal shape convolved with a Gaussian function to account for a possible difference in the mass resolution between data and MC simulation. The background events from e^+e^- annihilations are described by the shape obtained from the data taken at $\sqrt{s} = 3.773$ GeV, while the peaking background from $\psi(3686) \to \Lambda\bar{\Sigma}^0\pi^0$ is modeled with the MC simulation shape. In the fit, the contributions of these two background sources are fixed to the values discussed above. In addition, the nonpeaking background is parametrized by a first-order Chebychev function.

From the fit, shown in Fig. 2, we estimate 23.0 ± 6.3 $\Lambda\bar{\Lambda}\pi^0$ events with a statistical significance of 3.7σ which is evaluated by comparing the likelihood values with and without the π^0 signal included in the fit. The detection efficiency obtained from MC simulation events is 9.0% and these results are summarized in Table III.

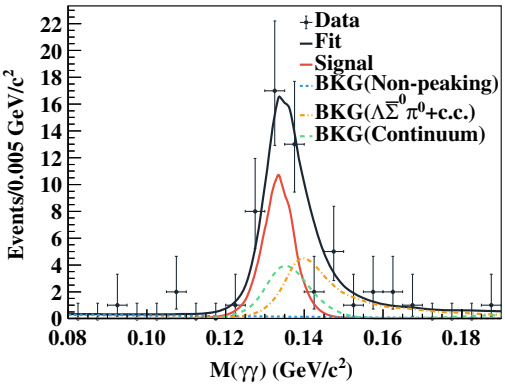

FIG. 2. The distribution of M$(\gamma\gamma)$ in the π^0 region. Dots with error bars are data, the black solid curve is the fit result, the red solid curve represents the signal, the blue dashed curve is the nonpeaking background, the orange dash-dotted solid curve is $\psi(3686) \to \Lambda\bar{\Sigma}^0\pi^0$, and the green long-dashed curve is the continuum background.

VI. ANALYSIS OF $\psi(3686) \to \Lambda\bar{\Lambda}\eta$

The distribution of $M(\gamma\gamma)$ in the η mass region is shown in Fig. 3. A fit to the η signal with the MC simulated signal shape convolved with a Gaussian function is performed, and the background contribution is described by the shape obtained from the continuum data plus a first order Chebychev function. The fitting results are shown in Fig. 3, with a total of 218 ± 17 $\Lambda\bar{\Lambda}\eta$ signal events.

To investigate possible intermediate states, M$(\gamma\gamma)$ is required to be in the η range $(0.525, 0.560)$ GeV$/c^2$. The resultant Dalitz plot of the 252 selected $\psi(3686) \to \Lambda\bar{\Lambda}\eta$ candidates, shown in Fig. 4, exhibits two visible clusters of events around $2.8(\mathrm{GeV}/c^2)^2$ in $\mathrm{M}^2(\eta\Lambda)$ and $\mathrm{M}^2(\eta\bar{\Lambda})$,

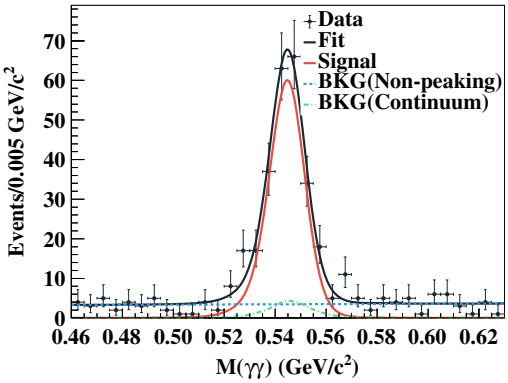

FIG. 3. The distribution of M$(\gamma\gamma)$ in the η mass region. Dots with error bars are data, the black solid curve is the fit result, the red solid curve represents the signal, the blue dashed curve is the nonpeaking background, and the green dash-dotted curve is the continuum background.

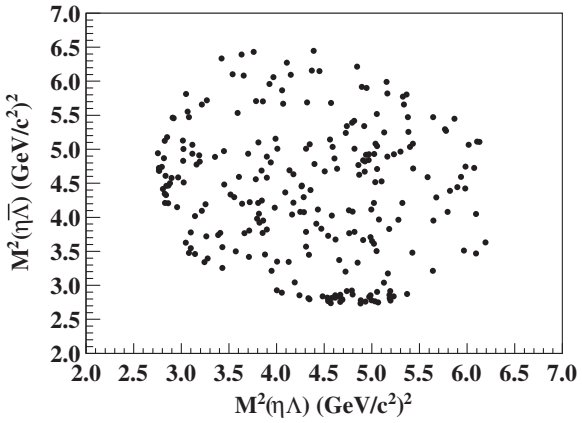

FIG. 4. The Dalitz plot of $M^2(\eta\Lambda)$ versus $M^2(\eta\bar{\Lambda})$.

indicating possible intermediate excited baryons. The invariant mass distributions of $M(\eta\Lambda)$ and $M(\eta\bar{\Lambda})$ presented in Figs. 5(a) and 5(b) show the corresponding structures. The η sidebands, $0.470\,\mathrm{GeV}/c^2 < M(\gamma\gamma) < 0.505\,\mathrm{GeV}/c^2$ and $0.580\,\mathrm{GeV}/c^2 < M(\gamma\gamma) < 0.615\,\mathrm{GeV}/c^2$, are used to estimate the number of background events; the obtained distributions, shown as shaded histograms in Figs. 5(a)–5(c), indicate that the structures are not from background events.

Using the Feynman diagram calculation package [22], a partial wave analysis (PWA) is performed based on an unbinned maximum likelihood fit. In the global fit, resonances are described by a relativistic Breit-Wigner propagator, with the mass and width as free parameters,

$$\mathrm{BW}(s) = \frac{1}{M^2_{\Lambda^*} - s - iM_{\Lambda^*}\Gamma_{\Lambda^*}}, \tag{1}$$

where s is the squared invariant mass.

To describe the $\Lambda\eta$ and $\bar{\Lambda}\eta$ mass spectra, all kinematically-allowed resonances of Λ^* and Σ^* listed in the PDG [14] are considered. Only components with a statistical significance larger than 5σ are kept in the baseline solution. PWA results indicate that the $\Lambda(1670)$ plus the nonresonant contribution could provide a good description of data, as illustrated in Figs. 5 and 6. The fitted mass and width of $\Lambda(1670)$, $(1672 \pm 5)\ \mathrm{MeV}/c^2$ and $(38 \pm 10)\ \mathrm{MeV}$, are also in agreement with the world average values; a total of $116 \pm 28\psi(3686) \to \Lambda(1670)\bar{\Lambda}$ candidate events are measured (based on the PWA amplitude "fit fraction"), and the detection efficiency is determined to be 12.5% by using a PWA-weighted MC sample. The measured yield and detection efficiency are summarized in Table III. The hypothesis of a $\Lambda(1690)$ state instead of $\Lambda(1670)$ in the model has been tested, leading to a reasonable description of the data, but with a sightly worse fit quality and with resonance parameters not consistent with the PDG values; it has thus been rejected.

To obtain the detection efficiency of $\psi(3686) \to \Lambda\bar{\Lambda}\eta$, a MC sample is generated in accordance with the above PWA results. The corrected detection efficiency, 12.9%, and the number of signal events, 218 ± 17 are presented in Table III.

VII. SYSTEMATIC UNCERTAINTIES

In this analysis, the systematic uncertainties on the branching fractions mainly come from the following sources:

(i) Λ reconstruction

The efficiency of $\Lambda(\bar{\Lambda})$ reconstruction is studied using the control sample of $\psi(3686) \to \Lambda\bar{\Lambda}$ decays, and a correction factor of 0.980 ± 0.011 [23] is applied to the efficiencies obtained from MC simulation. The uncertainty of the correction factor, 1.1%, which includes the uncertainties of MDC tracking and $\Lambda(\bar{\Lambda})$ reconstruction, is considered as the uncertainty of the efficiency of $\Lambda(\bar{\Lambda})$ reconstruction.

(ii) Photon detection

The photon detection efficiency has been studied using a high-purity control sample of $J/\psi \to \rho^0\pi^0$ [24]. The difference between the detection efficiencies of data and MC is around 1% per photon. Thus,

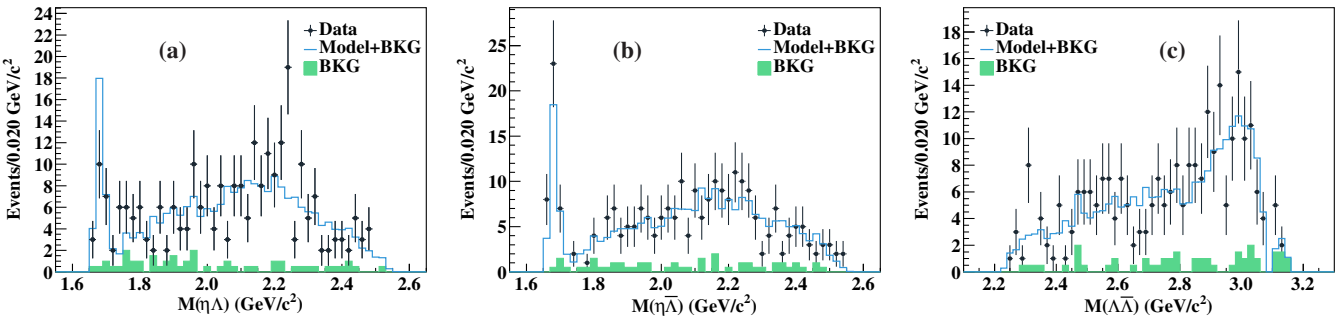

FIG. 5. The distributions of (a) $M(\eta\Lambda)$, (b) $M(\eta\bar{\Lambda})$, and (c) $M(\Lambda\bar{\Lambda})$. Dots with error bars represent data, the blue histograms are the sum of the PWA results and η sidebands, and the background contributions estimated from the η sidebands are indicated with the green shaded histograms.

2% is assigned as the total systematic uncertainty for the detection of the two photons.

(iii) Kinematic fit

The uncertainty associated with the 4C kinematic fit comes from the inconsistency between data and MC simulation in the fit. This difference is reduced by correcting the track helix parameters of the MC simulation, with parameters from [25,26]. Following the method described in Ref. [27], we obtain the systematic uncertainties of the 4C kinematic fit as 3.8% and 1.8% for $\psi(3686) \to \Lambda\bar{\Lambda}\pi^0$ and $\psi(3686) \to \Lambda\bar{\Lambda}\eta$, respectively.

(iv) Mass window requirements

The systematic uncertainties related to each individual mass window requirement are estimated by varying the size of the mass window by one standard deviation of the corresponding mass resolution. For the mass window of $\mathrm{M}(\Lambda\bar{\Lambda}) < 3.4\ \mathrm{GeV}/c^2$, the uncertainty is estimated by decreasing the required mass threshold by $10\ \mathrm{MeV}/c^2$. The largest variation of branching fraction for each mass requirement is considered as the related systematic uncertainty.

(v) Signal shape

In order to estimate the systematic uncertainty due to the signal shape, alternative fits are performed to determine the yields of signal events; the MC shape is replaced with a Breit-Wigner function convolved with a Gaussian function or a single Gaussian function, by varying the fits of the invariant mass distributions by either contracting, expanding or shifting the fit range by ± 10 MeV. The maximum differences with the nominal results are assigned as the corresponding systematic uncertainties.

(vi) Background uncertainty

To estimate the uncertainty of the nonpeaking background shape in the fit to $\mathrm{M}(\gamma\gamma)$, we performed alternative fits by replacing the first-order Chebychev function with a second-order Chebychev function for $\psi(3686)$ data. The maximum changes of 2.0% and 3.5% are considered as systematic uncertainties. The uncertainties of background from continuum events and the decay $\psi(3686) \to \bar{\Lambda}\Sigma^0\pi^0$ are propagated from the statistical uncertainties quoted in Sec. IV.

(vii) Interference between $\psi(3686)$ and continuum amplitudes

To estimate the effect from interference of the continuum amplitude with the resonance amplitude, we use the method from Ref. [28]. The maximum impact from interference term with respect to the resonance term is defined as $r_R^{\max}$,

$$r_R^{\max} = \frac{4}{\hbar c} AB, \qquad A = \sqrt{\frac{\sigma_c^f(s)}{\mathcal{B}_f}}, \tag{2}$$

where $\hbar c$ is the conversion constant, $\sigma_c^f(s)$ is the cross section of the continuum process measured from data, $\mathcal{B}_f$ is the branching fraction of $\psi(3686) \to \Lambda\bar{\Lambda}\pi^0$ and $\psi(3686) \to \Lambda\bar{\Lambda}\eta$ that we measured in this paper and the factor B is constant depending on the resonance parameters quoted from Ref. [28]. The $r_R^{\max}$, 40.3% and 20.6% of $\psi(3686) \to \Lambda\bar{\Lambda}\pi^0$ and $\psi(3686) \to \Lambda\bar{\Lambda}\eta$, are taken as the uncertainty of interference, respectively. Since the $\Lambda(1670)\bar{\Lambda}$ cannot be studied well in continuum with our current statistics, no systematic is provided for this final state.

(viii) Physics model

To have a good description of data from $\psi(3686) \to \Lambda\bar{\Lambda}\eta$, an event generator based on the PWA results is developed to determine the detection efficiency. We vary the default configuration to a setup either with only the $\Lambda(1690)$ or with a combination of $\Lambda(1670)$ and $\Lambda(1690)$, and consider the largest change in the detection efficiency as systematic uncertainty of the physical model. For $\psi(3686) \to \Lambda\bar{\Lambda}\pi^0$, we use PHSP as the nominal event generator. The change in detection efficiency using an alternative model within the allowed phase space of the $\Lambda\pi^0$ system resonances is assigned as systematic uncertainty for the $\Lambda\bar{\Lambda}\pi^0$ model.

(ix) Intermediate decays

The uncertainties of the quoted decay branching fractions for the intermediate particles from PDG [14] are taken as systematic uncertainties.

(x) Number of $\psi(3686)$ events

The number of $\psi(3686)$ events is determined from an analysis of inclusive hadronic $\psi(3686)$ decays. The uncertainty of the number of $\psi(3686)$ events, 0.6% [2], is taken as systematic uncertainty.

In addition, the systematic uncertainties associated with the PWA, which contribute to the measurement of the $\Lambda(1670)$ mass and width and of the corresponding production branching fraction, are described below.

(i) Additional resonances

To investigate the impact on the PWA results from other possible components, the analysis has been performed including additional possible states [e.g., $\Lambda(1690)$]. The changes of the mass, width, and fitted fraction of $\Lambda(1670)$ are considered as systematic uncertainties, and the largest one was chosen.

(ii) Background uncertainty

In the $\psi(3686) \to \Lambda\bar{\Lambda}\eta$ decays, the background level is quite low, and the events from the η sidebands are considered in the PWA. To estimate the uncertainty, the scale factor of background events from η sidebands has been varied by $\pm 50\%$, and the largest variation of the results is assigned as systematic uncertainty.

TABLE I. The systematic uncertainties for the (product) branching fractions of $\psi(3686) \to \Lambda\bar{\Lambda}\pi^0$, $\psi(3686) \to \Lambda\bar{\Lambda}\eta$ and $\psi(3686) \to \Lambda\bar{\Lambda}(1670)$. All values are given in percent.

Source	$\psi(3686) \to \Lambda\bar{\Lambda}\pi^0$	$\psi(3686) \to \Lambda\bar{\Lambda}\eta$	$\psi(3686) \to \Lambda\bar{\Lambda}(1670)$
$\Lambda(\bar{\Lambda})$ reconstruction	1.1[b]	1.1	1.1
Photon detection	2.0[b]	2.0	2.0
Kinematic fit	3.8[b]	1.8	1.8
Mass window requirements	7.1[b]	5.1	5.1
Signal shape	0.9[a]	1.2	...
Nonpeaking background	2.0[a]	3.5	...
Peaking background	7.3[a]	1.0	...
Interference between $\psi(3686)$ and continuum amplitudes	40.3[a]	20.6	...
Physics model	1.4[b]	3.4	...
$\mathcal{B}(\Lambda \to p\pi)$	0.8[b]	0.8	0.8
$\mathcal{B}(\pi^0(\eta) \to \gamma\gamma)$	0.03[b]	0.5	0.5
Number of $\psi(3686)$ events	0.6[b]	0.6	0.6
PWA additional resonances	...	...	34.2
PWA background	...	...	12.9
PWA PHSP parametrization	...	...	30.6
Total	41.9	22.1	48.0

[a]Additive.
[b]Multiplicative.

(iii) PHSP parametrization

In the partial wave analysis, PHSP is parametrized as a resonance with an extremely large width, and fixed values of spin and parity. The contribution to the systematic uncertainty is estimated by replacing the spin parity of $\frac{1}{2}^-$ with $\frac{1}{2}^+$, $\frac{3}{2}^-$, or $\frac{3}{2}^+$. The largest resulting difference is taken as systematic uncertainty.

All the systematic uncertainty sources and values are summarized in Tables I and II, respectively, for the $\psi(3686) \to \Lambda\bar{\Lambda}\pi^0$ and $\psi(3686) \to \Lambda\bar{\Lambda}\eta$ decays, where the total uncertainties are given by the quadratic sum, assuming statistical independence of all the contributions. The distinction between additive and multiplicative sources of systematic uncertainties are indicated in the table.

VIII. RESULTS

The branching fractions of the decays of interest are calculated as

$$\mathcal{B}(\psi(3686) \to \Lambda\bar{\Lambda}X) = \frac{N_X^{\rm obs}}{N_{\psi(3686)} \cdot \mathcal{B}^2(\Lambda \to p\pi^-) \cdot \mathcal{B}(X \to \gamma\gamma) \cdot \epsilon}, \quad (3)$$

where X is π^0 or η, $N_X^{\rm obs}$ is the number of signal candidates, $N_{\psi(3686)}$ is the number of $\psi(3686)$ events determined with inclusive hadronic events, ϵ is the detection efficiency obtained from the MC simulation. $\mathcal{B}(\Lambda \to p\pi^-)$, $\mathcal{B}(\pi^0 \to \gamma\gamma)$ and $\mathcal{B}(\eta \to \gamma\gamma)$ are the corresponding branching fractions from PDG [14]. Using the numbers given in Table III, the branching fractions of $\psi(3686) \to \Lambda\bar{\Lambda}\pi^0$ and $\psi(3686) \to \Lambda\bar{\Lambda}\eta$ are measured to be $\mathcal{B}(\psi(3686) \to \Lambda\bar{\Lambda}\pi^0) = (1.42 \pm 0.39 \pm 0.59) \times 10^{-6}$ and $\mathcal{B}(\psi(3686) \to \Lambda\bar{\Lambda}\eta) = (2.34 \pm 0.18 \pm 0.52) \times 10^{-5}$, respectively, where the first uncertainties are statistical and the second systematic.

Based on the PWA results, it was found that the evident structure around the $\Lambda\eta$ mass threshold could be described by the $\Lambda(1670)$. The mass and width are determined to be $\mathrm{M} = (1672 \pm 5 \pm 6)$ MeV/c^2 and

TABLE II. Summary of the systematic uncertainty sources contributing to the mass (ΔM) and width ($\Delta\Gamma$) of $\Lambda(1670)$.

Source	ΔM(MeV/c^2)	$\Delta\Gamma$(MeV)
PWA Additional resonances	6	12
PWA Background	2	2
PWA PHSP parametrization	1	14
Total	6	19

TABLE III. Summary of the signal yields and detection efficiencies for each decay mode.

Decay modes	$N^{\rm obs}$	ϵ(%)
$\psi(3686) \to \Lambda\bar{\Lambda}\pi^0$	23.0 ± 6.3	9.0
$\psi(3686) \to \Lambda\bar{\Lambda}\eta$	218 ± 17	12.9
$\psi(3686) \to \Lambda(1670)\bar{\Lambda}$	116 ± 28	12.5

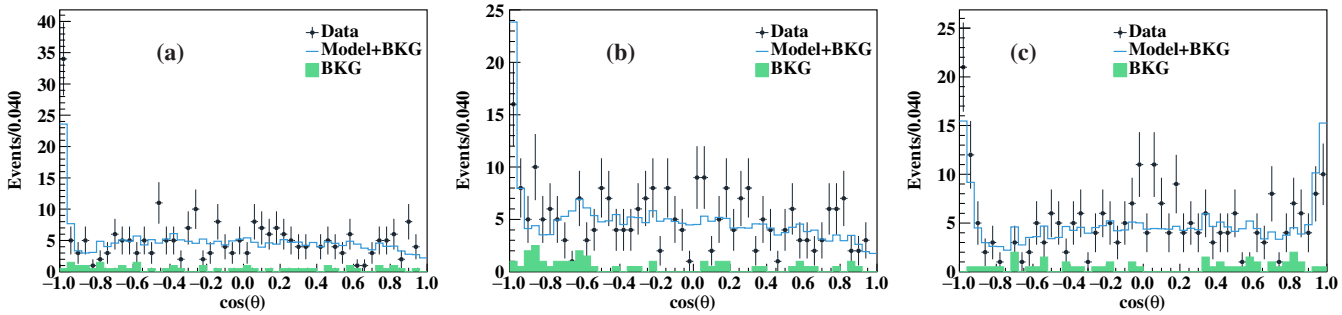

FIG. 6. The distributions of (a) $\cos\theta$ between Λ and $\bar{\Lambda}$ in the center-of-mass system (CMS) of $\eta\Lambda$, (b) $\cos\theta$ between Λ and $\bar{\Lambda}$ in CMS of $\eta\bar{\Lambda}$ and (c) $\cos\theta$ between η and Λ in CMS of $\Lambda\bar{\Lambda}$. The dots with error bars represent data, the blue histograms are the sum of the PWA results and η sidebands, and the green shaded histograms are the background events from η sidebands.

$\Gamma = (38 \pm 10 \pm 19)$ MeV, which are consistent with those in PDG [14]. The corresponding product branching fraction is calculated to be $\mathcal{B}(\psi(3686) \to \Lambda(1670)\bar{\Lambda}) \times \mathcal{B}(\Lambda(1670) \to \Lambda\eta) = (1.29 \pm 0.31 \pm 0.62) \times 10^{-5}$, where the first uncertainty is statistical and the second is systematic.

Due to the limited statistical significance of the $\psi(3686) \to \Lambda\bar{\Lambda}\pi^0$ signal (3.7σ), the upper limit of this branching fraction has been determined. We repeat the maximum-likelihood fits by varying the signal shape, nonpeaking background, peaking background as well as interference between $\psi(3686)$ and continuum amplitudes, and take the most conservative upper limit among different choices. To incorporate the multiplicative systematic uncertainties in the calculation of the upper limit, the likelihood distribution is smeared by a Gaussian function with a mean of zero and a width equal to σ_ϵ as shown below [29,30]

$$L'(n') \propto \int_0^\infty L\left(n\frac{\epsilon}{\epsilon_0}\right) \exp\left[\frac{-(\epsilon-\epsilon_0)^2}{2\sigma_\epsilon^2}\right] d\epsilon, \qquad (4)$$

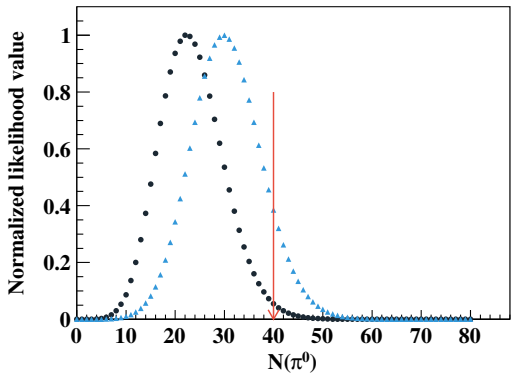

FIG. 7. The normalized likelihood distributions. The results obtained with and without incorporating the systematic uncertainties are shown in blue dots and black dots, respectively. The arrow is the position of the upper limit on the signal yields at 90% CL.

where $L(n)$ is the likelihood distribution as a function of the yield n, ϵ_0 is the detection efficiency and σ_ϵ is the multiplicative systematic uncertainty. Figure 7 shows the likelihood function without and with incorporating the systematic uncertainties. The upper limit on the number of $\psi(3686) \to \Lambda\bar{\Lambda}\pi^0$ events, N'_{UL}, is determined to be 40, and the corresponding upper limit of the branching fraction is obtained to be $\psi(3686) \to \Lambda\bar{\Lambda}\pi^0 < 2.47 \times 10^{-6}$ at the 90% CL.

IX. SUMMARY

Using a sample of $448.1 \times 10^6 \psi(3686)$ events collected with BESIII detector at the peak of $\psi(3686)$, we performed a study of $\psi(3686) \to \Lambda\bar{\Lambda}\pi^0$ and $\psi(3686) \to \Lambda\bar{\Lambda}\eta$.

Evidence of the isospin symmetry breaking decay of $\psi(3686) \to \Lambda\bar{\Lambda}\pi^0$ is observed with a statistical significance of 3.7σ, and the corresponding branching fraction is measured to be $\mathcal{B}(\psi(3686) \to \Lambda\bar{\Lambda}\pi^0) = (1.42 \pm 0.39 \pm 0.59) \times 10^{-6}$ for the first time. The corresponding upper limit at the 90% CL is set to be $\mathcal{B}(\psi(3686) \to \Lambda\bar{\Lambda}\pi^0) < 2.47 \times 10^{-6}$.

In the case of $\psi(3686) \to \Lambda\bar{\Lambda}\eta$, a PWA is performed to investigate the observed structure around $\Lambda\eta(\bar{\Lambda}\eta)$. This structure can be described by a $\Lambda(1670)$ with $M = (1672 \pm 5 \pm 6)$ MeV/c^2 and $\Gamma = (38 \pm 10 \pm 19)$ MeV, which are in good agreement with those reported by PDG [14]. The corresponding product branching fraction is calculated to be $\mathcal{B}(\psi(3686) \to \Lambda(1670)\bar{\Lambda}) \times \mathcal{B}(\Lambda(1670) \to \Lambda\eta) = (1.29 \pm 0.31 \pm 0.62) \times 10^{-5}$. With the detection efficiency obtained from the weighted MC sample in accordance with the PWA results, the branching fraction of $\psi(3686) \to \Lambda\bar{\Lambda}\eta$ is measured to be $\mathcal{B}(\psi(3686) \to \Lambda\bar{\Lambda}\eta) = (2.34 \pm 0.18 \pm 0.52) \times 10^{-5}$.

Compared with the branching fraction of $J/\psi \to \Lambda\bar{\Lambda}\pi^0$ and $J/\psi \to \Lambda\bar{\Lambda}\eta$ [1], the ratio between the branching fractions of $\psi(3686)$ and J/ψ decaying to the same hadronic final state is defined as $\mathcal{Q}_h$. Taking PHSP factors into account, the ratio of $\Lambda\bar{\Lambda}\pi^0$ and $\Lambda\bar{\Lambda}\eta$, $\mathcal{Q}_h(\pi^0)$ and

$\mathcal{Q}_h(\eta)$, are calculated to be $(1.4 \pm 0.7)\%$ and $(2.3 \pm 0.6)\%$, respectively, both contradicting the 12% rule significantly.

ACKNOWLEDGMENTS

The BESIII collaboration thanks the staff of BEPCII and the IHEP computing center for their strong support. This work is supported in part by National Key Reseach and Development Program of China under Contracts Nos. 2020YFA0406300, 2020YFA0406400; the Chinese Academy of Sciences (CAS) Large-Scale Scientific Facility Program; Joint Large-Scale Scientific Facility Funds of the NSFC and CAS under Contract No. U2032110; National Natural Science Foundation of China (NSFC) under Contracts No. 11635010, No. 11735014, No. 11835012, No. 11935015, No. 11935016, No. 11935018, No. 11961141012, No. 12022510, No. 12025502, No. 12035009, No. 12035013, No. 12192260, No. 12192261, No. 12192262, No. 12192263, No. 12192264, and No. 12192265; CAS Key Research Program of Frontier Sciences under Contract No. QYZDJ-SSW-SLH040; 100 Talents Program of CAS; INPAC and Shanghai Key Laboratory for Particle Physics and Cosmology; ERC under Contract No. 758462; European Union's Horizon 2020 research and innovation program under Marie Sklodowska-Curie grant agreement under Contract No. 894790; German Research Foundation DFG under Contracts No. 443159800, Collaborative Research Center CRC 1044, GRK 2149; Istituto Nazionale di Fisica Nucleare, Italy; Ministry of Development of Turkey under Contract No. DPT2006K-120470; National Science and Technology fund; STFC (United Kingdom); The Royal Society, UK under Contracts No. DH140054, and No. DH160214; The Swedish Research Council; U.S. Department of Energy under Contract No. DE-FG02-05ER41374.

[1] M. Ablikim *et al.* (BESIII Collaboration), Measurements of the branching fractions for J/ψ and $\psi' \to \Lambda\bar{\Lambda}\,\pi^0$ and $\Lambda\bar{\Lambda}\eta$, Phys. Rev. D **87**, 052007 (2013).
[2] M. Ablikim *et al.* (BESIII Collaboration), Determination of the number of $\psi(3686)$ events at BESIII, Chin. Phys. C **42**, 023001 (2018).
[3] A. Duncan and A. H. Mueller, Heavy quarkonium decays and the renormalization group, Phys. Lett. **93B**, 119 (1980).
[4] S. J. Brodsky and G. P. Lepage, Helicity selection rules and tests of gluon spin in exclusive QCD processes, Phys. Rev. D **24**, 2848 (1981).
[5] V. L. Chernyak and A. R. Zhitnitsky, Exclusive decays of heavy mesons, Nucl. Phys. **B201**, 492 (1982).
[6] M. Ablikim *et al.* (BESIII Collaboration), Design and construction of the BESIII detector, Nucl. Instrum. Methods Phys. Res., Sect. A **614**, 345 (2010).
[7] C. Yu *et al.*, in *Proceedings of the 7th International Particle Accelerator Conference*, International Particle Accelerator Conference (JACoW, Geneva, Switzerland, 2016), p. TUYA01, 10.18429/JACoW-IPAC2016-TUYA01.
[8] M. Ablikim *et al.* (BESIII Collaboration), Future physics programme of BESIII, Chin. Phys. C **44**, 040001 (2020).
[9] S. Agostinelli *et al.* (GEANT4 Collaboration), GEANT4—a simulation toolkit, Nucl. Instrum. Methods Phys. Res., Sect. A **506**, 250 (2003).
[10] S. Jadach, B. F. L. Ward, and Z. Was, Coherent exclusive exponentiation for precision Monte Carlo calculations, Phys. Rev. D **63**, 113009 (2001).
[11] S. Jadach, B. F. L. Ward, and Z. Was, The precision Monte Carlo event generator KK for two fermion final states in e^+e^- collisions, Comput. Phys. Commun. **130**, 260 (2000).
[12] D. J. Lange, The EvtGen particle decay simulation package, Nucl. Instrum. Methods Phys. Res., Sect. A **462**, 152 (2001).
[13] R.-G. Ping, Event generators at BESIII, Chin. Phys. C **32**, 599 (2008).
[14] R. L. Workman (Particle Data Group), Review of particle physics, Prog. Theor. Exp. Phys. **2022**, 083C01 (2022).
[15] J. C. Chen, G. S. Huang, X. R. Qi, D. H. Zhang, and Y. S. Zhu, Event generator for J/ψ and $\psi(2S)$ decay, Phys. Rev. D **62**, 034003 (2000).
[16] R.-L. Yang, R.-G. Ping, and H. Chen, Tuning and validation of the lundcharm model with J/ψ decays, Chin. Phys. Lett. **31**, 061301 (2014).
[17] E. Richter-Was, QED bremsstrahlung in semileptonic B and leptonic τ decays, Phys. Lett. B **303**, 163 (1993).
[18] M. Xu *et al.*, Decay vertex reconstruction and 3-dimensional lifetime determination at BESIII, Chin. Phys. C **33**, 428 (2009).
[19] X. Zhou, S. Du, G. Li, and C. Shen, TopoAna: A generic tool for the event type analysis of inclusive Monte-Carlo samples in high energy physics experiments, Comput. Phys. Commun. **258**, 107540 (2021).
[20] M. Ablikim (BESIII Collaboration), Measurement of the integrated luminosities of the data taken by BESIII at $\sqrt{s} = 3.650$and 3.773 GeV, Chin. Phys. C **37**, 123001 (2013).
[21] D. M. Asner *et al.*, Physics at BES-III, Int. J. Mod. Phys. A **24**, S1 (2009), https://inspirehep.net/literature/796263.
[22] J.-X. Wang, Progress in FDC project, Nucl. Instrum. Methods Phys. Res., Sect. A **534**, 241 (2004).
[23] M. Ablikim *et al.* (BESIII Collaboration), Study of J/ψ and $\psi(3686)$ decay to $\Lambda\bar{\Lambda}$ and $\Sigma^0\bar{\Sigma}^0$ final states, Phys. Rev. D **95**, 052003 (2017).
[24] M. Ablikim *et al.* (BESIII Collaboration), Study of χ_{cJ} radiative decays into a vector meson, Phys. Rev. D **83**, 112005 (2011).

[25] M. Ablikim *et al.* (BESIII Collaboration), Search for $\eta_c(2s)h_c \to p\bar{p}$ decays and measurements of the $\chi_{cJ} \to p\bar{p}$ branching fractions, Phys. Rev. D **88**, 112001 (2013).
[26] M. Ablikim *et al.* (BESIII Collaboration), Cross section measurements of $e^+e^- \to \omega\chi_{c0}$ form $\sqrt{s} = 4.178$ to 4.278 GeV, Phys. Rev. D **99**, 091103 (2019).
[27] M. Ablikim *et al.* (BESIII Collaboration), Search for hadronic transition $\chi_{cJ} \to \eta_c\pi^+\pi^-$ and observation of $\chi_{cJ} \to K\bar{K}\pi\pi\pi$, Phys. Rev. D **87**, 012002 (2013).
[28] Y. P. Guo and C. Z. Yuan, Impact of the interference between the resonance and continuum amplitudes on vector quarkonia decay branching fraction measurements, Phys. Rev. D **105**, 114001 (2022).
[29] K. Stenson, A more exact solution for incorporating multiplicative systematic uncertainties in branching ratio limits, arXiv:physics/0605236.
[30] X.-X. Liu, X.-R. Lü, and Y.-S. Zhu, Combined estimation for multi-measurements of branching ratio, Chin. Phys. C **39**, 103001 (2015).

Correction: An error introduced during the production process in the Collaboration name has been set right.